The interaction between mucin and poly(amino acid)s with controlled cationic group content in bulk phase and in thin layers

Gergely Stankovits[1], Ágnes Ábrahám[2,3], Éva Kiss[2], Zoltán Varga[1,4], Anil Misra[5], András Szilágyi[1], Benjámin Gyarmati[1*]*

[1]Department of Physical Chemistry and Materials Science, Faculty of Chemical Technology and Biotechnology, Budapest University of Technology and Economics, Műegyetem rkp. 3., H-1111 Budapest, Hungary

[2]Laboratory of Interfaces and Nanostructures, Institute of Chemistry, Eötvös Loránd University, Pázmány Péter Sétány 1/A, H-1117 Budapest, Hungary

[3]MTA-TTK Lendület "Momentum" Peptide-Based Vaccines Research Group, Institute of Materials and Environmental Chemistry, Research Centre for Natural Sciences, H-1117 Budapest, Magyar Tudósok Krt. 2.

[4]Research Centre for Natural Sciences, Institute of Materials and Environmental Chemistry, Magyar tudósok körútja 2, 1117 Budapest, Hungary

[5]Pharmidex Pharmaceutical Services, Office 3.05, 1 King Street, London, EC2V 8AU, United Kingdom

Corresponding Authors

*E-mail: szilagyi.andras@vbk.bme.hu; gyarmati.benjamin@vbk.bme.hu

KEYWORDS

mucoadhesion, adsorption, quartz crystal microbalance

Highlights

- Cationic polyaspartamides with controlled cationic group content were synthesised
- The strength of mucin-polymer interactions changed non-linearly with composition
- The highest adsorption was at intermediate cationic side group content shown by QCM
- A close correlation was found between the bulk (3D) and thin layer (2D) interactions

GRAPHICAL ABSTRACT

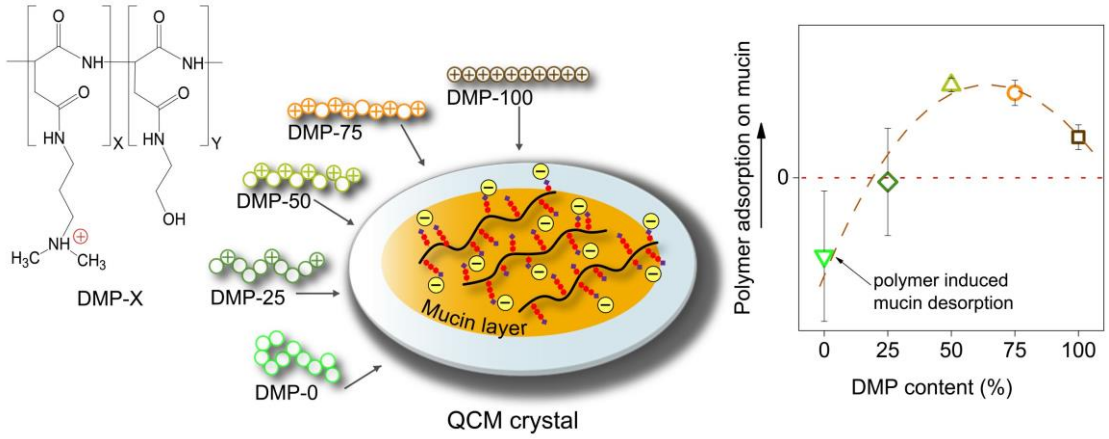

ABSTRACT

The type and concentration of charged groups in polymers have a key role in mucoadhesive interactions. A series of cationic poly(amino acid)s with different charge densities was designed to unravel the correlation between chemical structure and mucin-polymer interactions. Colloidal interactions between the mucin protein and synthetic polyaspartamides were tested by dynamic light scattering, zeta potential measurements and turbidimetric titration as a function of polymer-to-mucin mass ratio. The mucoadhesive interactions displayed a strongly non-linear change with polymer composition. The attractive interactions between mucin and the polyaspartamides with at least 50% cationic groups caused increased light scattering of dispersions due to the aggregation of mucin particles upon their charge reversal. Interactions were further analysed in a thin mucin layer to model life-like situations using a quartz crystal microbalance (QCM) in flow mode. Results pointed out that the fully cationic polyaspartamide is not necessarily superior to derivatives with lower cationic group content. The maximum of adsorbed mass of polymers on mucin was experienced at medium cationic group contents. This emphasizes the relevance of cationic polyaspartamides as mucoadhesive excipients due to their multiple functionalities and the possibility of fine-tuning their interactions with mucin via straightforward chemical steps.

1. INTRODUCTION

Mucosal surfaces are important targets for drug formulations as they provide high permeability and enable avoiding first-pass metabolism [1]. The two main concepts for utilising these surfaces are mucoadhesion and mucopenetration; both require the fine-tuning of colloidal interactions between the polymer excipient(s) of the formulations and the mucin proteins, the major component of the mucus secreted by the mucosa. The attractive interactions must be maximised to achieve mucoadhesion, whereas mucopenetration requires the exclusion of those interactions, so the drug formulation can pass through the mucus and reach the deeper layers. These two concepts should not be considered separately, but rather as complementary approaches to improve therapeutic efficiency [2]–[5]. It is also possible to achieve a synergistic effect by their combination, e.g., by the embedment of mucopenetrating nanoparticles in a mucoadhesive film for buccal delivery [4]. Understanding the prevailing interactions between the polymer component and mucin is a core question in formulation development. The factors influencing the strength of mucoadhesive interactions are scarcely reported, and only a few papers exist on such structure-function relationships [6], [7]. Many structural properties (e.g., molecular mass, functional groups, cross-linking, branching and conformation) and external conditions (pH, ionic strength, the amount of water on the target size) influence the mucoadhesive and mucopenetrating performance of polymers [8], [9]. Still it is generally accepted that electrostatic interactions play a significant role in several cases [10]–[16]. Cationic polymers are expected to develop attractive interactions with the anionic mucin glycoprotein and thus are considered important mucoadhesive excipients. Chitosan is the most studied representative on which the effect of molecular mass [17] and the chemical structure on the mucoadhesive interactions have been studied in some papers [18]–[21]. The partial elimination of amine groups of chitosan affected the strength of electrostatic interactions but also weakened hydrogen bonding and hydrophobic interactions in a complex

way. However, the effect of chemical functionality on interactions was not studied on a detailed composition scale by Sogias et al. [19]. Stie et al. showed that chitosans with various acetylation degrees displayed structure-dependent interaction strength with mucin in thin layers suggesting the importance of concentration of amine groups, but the nature of interactions was not analysed [20]. As a more systematic study on synthetic polymers, Fefelova et al. investigated the role of cationic co-monomer content of amphiphilic polyacrylamides in mucoadhesive interactions. As the polymers studied contained predominantly hydrophobic side groups, minor effects of the cationic co-monomers were obtained because mucin-polymer interactions were mainly determined by the hydrophobic association [21]. It can be concluded that no systematic study has yet been reported on the role of charge density in the strength of mucoadhesion, including hydrophilic polymers. It is known that the charge density of polymers strongly affects their conformation; e.g., it can change the conformation of the polymer from a random coil to a rod-like structure that determines whether the polymer adsorbs on an oppositely charged surface. [22]. There are only a few models and experimental results on how the polymer charge density determines the structure and the strength of interactions between the polymers and oppositely charged macroions, spherical particles or planar surfaces. It is proven that the enthalpy of adsorption of polymers increases with charge density [22]–[24]. Such a trend, probably due to the complex chemical structure and conformation variability of mucin proteins, has yet to be established for interactions with mucin-covered surfaces or in mucin dispersions [25], [26].

Polymer-mucin interactions are mainly studied by colloidal methods using dilute mucin dispersions. These methods are usually based on the analysis of scattered light from interacting macromolecules, such as in turbidimetric titration and dynamic light scattering (DLS) measurements, which can provide quantitative information about the stoichiometry of interactions and indicate their nature and strength [10], [12], [27]. The use of dilute mucin

dispersions provides an opportunity for the formation of interactions in the bulk phase (3D), which does not mimic *in vivo* situations, where interactions are restricted to thin layers and considerable shear stress might be present on, e.g., ocular, intestinal or nasal surfaces. Quartz crystal microbalance (QCM) is a versatile tool to quantify adsorption on a thin layer in aqueous media. In addition to the adsorbed mass on a thin layer, the consistency of the adsorbed layer can also be deduced. Using QCM in a flow system is possible, so shear stress present in biological systems can also be modelled. Due to these advantages, QCM is commonly used for studying the interaction of biomacromolecules [28]–[32], but its application for mucin layers [33] has been reported only recently for a limited set of polymers [34], [35].

Our goal is to reveal the role of charge density in mucin-polymer interactions both in dispersion and in thin layers. To this end, the class of polyaspartamides was chosen because of their chemical versatility, biocompatibility and biodegradability [36]–[39]. A series of cationic polyaspartamides with identical backbone length and controlled charge density was synthesised. The two ends of the compositional scale were the completely neutral polyaspartamide and its fully cationic counterpart. The adsorption of polyaspartamides on mucin was monitored through the polymer-induced colloidal aggregation of mucin, with the resulting elevated light scattering as an indicator of interactions. The role of charges in mucin aggregation was analysed by zeta potential measurements. As a better model of *in vivo* situations, polymer adsorption was further studied on thin layers composed of mucin by QCM to compare the binding affinity of polyaspartamides. An attempt was made to correlate the interactions in the bulk phase and thin layers.

2. MATERIALS AND METHODS

2.1. Materials

Mucin (from porcine stomach, type II), L-aspartic acid (99.5%), phosphoric acid (99%), 3-(dimethylamino)-1-propylamine (DMP, 99%), ethanolamine (HE, 99%), Triton X-100 (AR), deuterium oxide (D_2O, 99.9 atom% D, contains 0.05 wt.% 3-(trimethylsilyl)propionic-2,2,3,3-d_4 acid, sodium salt) and dialysis tubing cellulose membrane (avg. flat width 76 mm, molecular weight cut-off 14 000 Da) were purchased from Merck. *N,N*-dimethylformamide (DMF, 100%) sodium chloride (NaCl), potassium chloride (KCl), dibasic sodium phosphate dihydrate ($Na_2HPO_4 \cdot 2\ H_2O$), monobasic potassium phosphate (KH_2PO_4), sodium acetate, acetic acid (96%) and hydrochloric acid (HCl; 37% AR) were bought from Reanal, Hungary. Ethyl acetate (99%), ammonia (25% aqueous solution, analytical grade), hydrogen peroxide (30% aqueous solution, analytical grade) and acetone (99%) were bought from Molar Chemicals. Ultrapure water (ρ > 18.2 MΩ cm, Millipore) was used for the preparation of buffer solutions. All reagents were used without any purification. Unless otherwise stated, all experiments were performed at 25 °C, in three parallels.

Phosphate-buffered saline (PBS) solution of pH = 7.4 was prepared by dissolving 8.00 g of NaCl, 0.20 g of KCl, 1.44 g of $Na_2HPO_4 \cdot 2\ H_2O$ and 0.12 g of KH_2PO_4 in 1 L of water, the pH was adjusted with 1 mol L^{-1} HCl and checked with a Mettler Toledo InLab®413 pH electrode.

Acetic acid/sodium acetate buffer (pH = 4.5, I = 0.5 M) was prepared by dissolving 33.34 g sodium acetate trihydrate and 22.97 g acetic acid in 1 L of water. The ionic strength of the buffer solution was adjusted to 0.5 M with 14.89 g of NaCl.

2.2 Synthesis of cationic polyaspartamides with controlled charge density

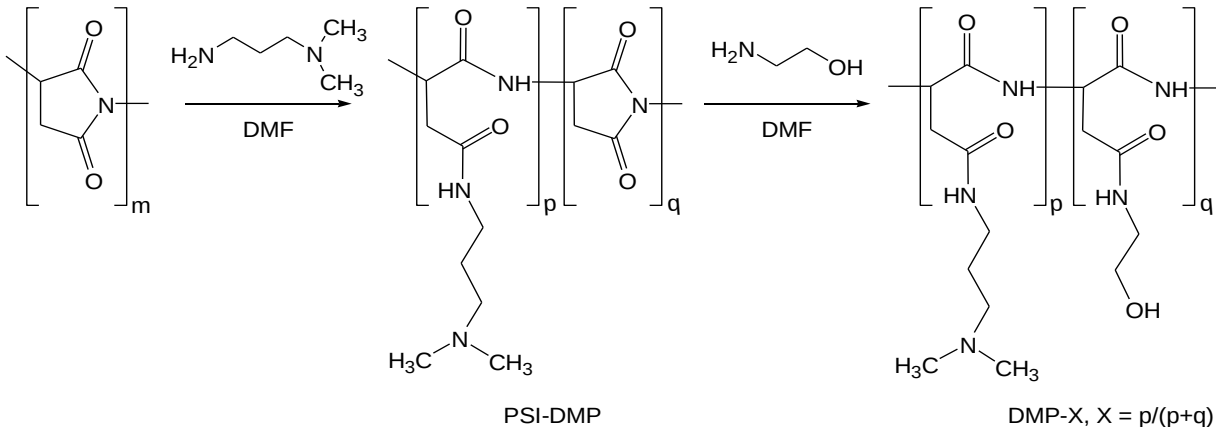

Scheme 1 The synthesis scheme of polyaspartamides (m = p+q); for the neutral derivative, the first step is omitted (p = 0)

Polysuccinimide (PSI) was synthesised by thermal polycondensation of aspartic acid, as reported earlier [40]. 1 g of PSI (10.3 mmol of succinimide repeating units) was dissolved in 9 g DMF and reacted with DMP in a nucleophilic addition reaction to have the desired cationic side group (DMP) ratio (25, 50, 75, or 100% of all repeating units). The cationic polyaspartamides with different DMP content are referred to as DMP-X, where X means the molar percentage of DMP side groups of all repeating units. The remaining succinimide rings were reacted with ethanolamine in excess (1.5-fold molar excess to succinimide rings). The reaction mixture was stirred for 24 h after each step. Finally, the reaction mixture (ca. 10 mL) was precipitated in cold (5 °C) ethyl acetate (100 mL), then the precipitate was washed 3 times with ethyl acetate (3x100 mL) and 3 times with acetone (3x20 mL). Polymers from their free base forms were then converted into hydrochloride salts by dissolving the precipitate in 1 M HCl equimolar to the DMP groups and diluted with water to reach 10 mL. In case of the completely neutral polymer (DMP-0) 10 mL water was used for the dissolution. Aqueous polymer solutions were dialysed against water for several days with regular changes

of water until the conductivity dropped below 10 mS cm^{-1}, then freeze dried to yield a solid, off-white product with an average yield of 70%.

2.3 Chemical characterisation

The chemical structure of the DMP-X polymers was analysed by ^{1}H NMR spectroscopy (500 MHz, 16 scans). 20 g L^{-1} solutions were prepared from freeze-dried polymers in D_2O.

2.4 Size exclusion chromatography

The number averaged molecular weight (M_n), weight averaged molecular weight (M_w), and polydispersity index (PDI) of the synthesised polyaspartamides were determined using size exclusion chromatography (SEC). A Jasco HPLC system (Jasco, Tokyo, Japan) consisting of a PU-4180 pump was used with Nucleogel GFC-300-8 column as a stationary phase and acetic acid/sodium acetate buffer (pH = 4.5, I = 0.5 M) as a mobile phase with a flow rate of 1 mL min^{-1}. A JASCO FP-2020 fluorescent detector was used with an excitation wavelength of 280 nm and an emission wavelength of 340 nm. All polymers were dissolved in the acetic acid/sodium acetate buffer (pH = 4.5, I = 0.5 M) at a 2 mg mL^{-1} concentration and 50 µL of each sample was injected. β-Galactosidase, bovine serum albumin, and wheat germ agglutinin (all purchased from Merck) were used as protein standards to estimate the molar mass distribution and the hydrodynamic diameter of the polyaspartamides.

2.5 Potentiometric titration

10 mg of each DMP-X polymer was dissolved in 10 mL 0.01 M HCl and titrated with 0.1 M NaOH. The ionic strength was kept constant by adding 0.1 M NaCl to both the titrant and the sample solutions. An auto-titrator (Metrohm, 808 Titrando used with the software Tiamo, version 1.2) with a 12 mm pH glass electrode (Metrohm, Electrode Plus, filled with 3 M KCl) was used to perform the titrations. The pH glass electrode was calibrated using Certipur®

buffer solutions (pH = 4.01; 6.86; 9.18) and the factor of the titrant solution (0.1 M NaOH) was determined by titration with 0.1 M HCl diluted from 1 M HCl (Titrisol®, Merck). Titrations were carried out under magnetic stirring, N_2 bubbling and constant temperature (23 ± 1 °C). "Dynamic Equivalence Point Titration" mode with custom parameters (maximum signal drift: 3 mV min^{-1}, min. waiting time: 5 s, max. waiting time: 40 s after each addition, min. volume increment 10 µL, max. volume increment 50 µL, finish at pH = 11.5) was used, all measurements were performed in triplicate. The molar amount of bound protons to the basic group (-N$(CH_3)_2$) was determined by converting titration curves (Fig. 1a) to Bjerrum-type plots (Fig. 1b) using eqn. (1)

$$\text{eqn. (1)} \qquad n_H = (V_0 c_{HCl} - V_t c_{NaOH}) - ([H^+] - K_w[H^+]^{-1})(V_0 + V_t) + N_H$$

where n_H represents the molar amount of bound protons to the basic groups (-N$(CH_3)_2$) at the given pH, N_H is the molar amount of dissociable groups in the polymer, K_w is the ionic product of water, $[H^+]$ is the hydrogen ion concentration, V_0 and V_t are the initial sample volume and the volume of the added titrant, respectively, and c_{HCl} and c_{NaOH} are the molar concentrations of HCl in sample and NaOH in the titrant, respectively.

2.6 Haemolysis assay

A haemolysis assay was carried out to determine the disruption of red blood cells upon contact with cationic polyaspartamides, in a similar manner as reported earlier [41]. In brief, the polymers and Triton-X-100 as the positive standard were tested at a final concentration of 1 g L^{-1} in PBS, while PBS was used as the negative control. Heparinised blood was obtained from male Sprague-Dawley (SD) rats by cardiac puncture under anaesthesia. The blood was kept on ice until used. Blood was used undiluted without any centrifugation, washing or other further treatments. The assay was performed in Eppendorf test tubes. 30 µL of samples and 270 µL of pure blood was added to each tube. Tubes were very gently mixed to avoid any

natural (non-assay induced) haemolysis. All tubes were then incubated at 37 °C for four hours. After incubation, samples were centrifuged at 1,000 G for 10 min. 100 µL of the supernatant from the samples was carefully pipetted (not to touch the pellet on the bottom of the tubes (red blood cells)) into the wells of a clear, flat bottom 96-well plate. A slight red colour was observed in some samples, indicating the presence of haemolysis. Absorbance was read at 540 nm with a Tecan Safire 2 plate reader. The results were calculated as a percentage of the complete haemolysis (Triton X-100 haemolysis = 100%).

2.7 Preparation of mucin dispersions and polymer solutions

Mucin dispersions for turbidimetry, dynamic light scattering (DLS), zeta potential and quartz crystal microbalance (QCM) measurements were prepared by dispersing mucin in 40 mL PBS buffer solution (pH = 7.4) at a concentration of 1 g L^{-1}. The dispersion was stirred for 2 h, sonicated for 10 min, centrifuged at 170 G for 5 min and the supernatant (maximum volume of 20 mL) was used for turbidimetric titrations. For DLS, zeta potential and QCM measurements, the supernatant was diluted tenfold with PBS solution and filtered through a glass filter with a pore size of 1.2 µm. DMP-X polymers were dissolved in PBS buffer solution (pH = 7.4) by gentle shaking for 10 min. The final polymer concentration was 1 g L^{-1} for turbidimetric titration, while a concentration of 0.1 g L^{-1} was used for DLS and zeta potential measurements. For QCM measurements both 1 g L^{-1} and 0.1 g L^{-1} concentrations were tested.

2.8 Turbidimetric titration

Turbidimetric titrations were performed to detect the colloidal interactions between mucin particles and DMP-X polymers. Each polymer solution was added stepwise into 2 mL of mucin dispersion. After each step, the solution was mixed gently for 10 s before the turbidity (apparent absorbance at 400 nm) was measured. Since the mucin dispersion itself is turbid,

the absorbance values of the blank titration of mucin dispersion with PBS solution were subtracted from each titration curve. The contribution of polymer-mucin interaction to turbidity was used further to analyse interactions.

2.9 Dynamic light scattering and zeta potential measurements.

Dynamic light scattering and zeta potential measurements were performed to obtain insights into colloidal aggregation in mucin dispersion with DMP-X polymers. Zetasizer (Zetasizer ProBlue, Malvern Panalytical Ltd., Malvern, UK) equipped with a 'Dip' cell (ZEN1002) was used to measure the hydrodynamic diameter and zeta potential of the particles in the samples. 1 mL mucin dispersion was mixed with the necessary volume of 0.1 g L^{-1} DMP-X solution outside the cell for 10 s, then 1 mL from the mixture was transferred to a polystyrene cuvette, and both DLS and zeta potential were measured immediately. The general model was used for DLS analysis, and a fixed attenuator position (9) was chosen to obtain comparable light scattering intensities. Z-average particle size was used for comparing different polyaspartamides as the most robust parameter of DLS measurements (ISO 13321). The Smoluchowski model was used to calculate the zeta potential from the measured electrophoretic mobility.

2.10 Quartz crystal microbalance measurement

A thin layer of mucin was deposited on gold-coated quartz crystals and the adsorption of DMP-X polymers on the mucin layer was examined in a flow cell to characterise the mucoadhesion in 2D. A QCM200 device (Stanford Research Systems, Sunnyvale, CA, USA) was used with AT-cut quartz crystal with great mass sensitivity and a low temperature coefficient around room temperature. The flow cell was connected to a peristaltic pump applying a liquid flow rate of 0.2 mL min^{-1} suggested by the manufacturer [42]. Experiments were performed at 25.0 ± 0.1 °C. The crystal had a resonant frequency of 5 MHz, while the

diameter, the sensitivity factor (C_f) and the inductance of the electrode were 14 mm, 56.6 Hz cm^2 μg^{-1} and 0.03 H, respectively.

A new QCM gold crystal sensor was used for each polymer, but the same sensor was used after cleaning for parallel measurement from the same polymer. Sensor crystal was cleaned by immersion into a 1:1:5 solution of hydrogen peroxide (30%), ammonia (25%) and water for 5 min. The purification process was followed by washing with water. Prior to each measurement, the sensor crystal was rinsed with acetone, ethanol and water, and finally treated in an air plasma chamber (30 W, 0.2 mbar) for 10 min.

During the measurements, the resonance frequency (f) and the motional resistance (R) of the sensor crystal were recorded. From the change in the frequency to the fundamental frequency (f_0), the mass adsorbed on the sensor crystal was calculated using eqn. 2. The mucin layer thickness was estimated from the adsorbed mass, the sensor surface area and the density of the adsorbed mucin layer ($\rho \approx 1$ g cm^{-3}). For each polymer, measurements were performed at least in duplicate.

eqn. 2. $$\Delta f = -\frac{2 f_0^2}{\sqrt{\mu_q \rho_q}} \Delta m = -C_f \Delta m$$

where f_0 fundamental frequency of the crystal, ρ_q and μ_q are the density and elastic modulus of quartz, respectively; C_f is the integral sensitivity or device constant comprising of the latter three constants, while Δm is the change in mass uniformly distributed on the active surface [43].

2.11 Atomic Force Microscopy

The deposition of a thin mucin layer on a gold-coated QCM crystal was studied with atomic force microscopy using a FlexAFM microscope system (Nanosurf AG, Liestal, Switzerland),

operating in dynamic mode. After mucin deposition, the crystal was removed from the flow cell and dipped three times into water shortly to remove salts, then dried in a desiccator using a low vacuum (approx. 16 mbar). Tap150GD-G cantilever (BudgetSensors Ltd., Sofia, Bulgaria) with a nominal tip radius of less than 10 nm was used for the measurements. Images were recorded over a 5 µm x 5 µm window areas at 10 randomly selected locations with a resolution of 512 pixels/line. Representative line profiles have been extracted from the images to characterize the surface roughness of the samples. The method of calculations can be found in Supplementary Data, Section 4.

2.12 Statistical analysis

TIBCO Statistica® 14.1.0 software was used for statistical analysis. Results from the haemolysis assay for DMP-X polymers (Section 3.3) were compared with the negative control using Dunnett's test, with the following alternative hypothesis: the expected haemolytic effect of a polymer is smaller than 1% compared to the negative control. The type II error was set to 0.05, presented by one-sided, 95% confidence intervals for each polymer. Thus, the alternative hypothesis can be accepted if the upper limit of the confidence interval is smaller than 1%. From turbidimetry tests (Section 3.4), each characteristic value: tg δ, turbidity at the initial increase and the maximum, as well as the corresponding mass ratios for DMP-X polymers were compared using multivariate ANOVA (MANOVA) test, considering each characteristic value as dependent variables. Tukey HSD post-hoc analysis was carried out for each dependent variable. In the case of QCM measurements (Section 3.5), a repeated measures ANOVA analysis was used to analyse the effect of the polymer composition and the different experimental stages on the polymer/mucin mass ratio. Different stages (at polymer concentrations of 0.1 g $L^{-1}$and 1 g L^{-1}, and after the second rinsing step) were taken as within-subject factor and polymer composition as between-subject factor. Sphericity of the model was proven by Mauchly sphericity test. Tukey HSD post-hoc tests were carried out to

compare both the stages and the polymer compositions. A level of $p \leq 0.05$ was taken as significant for all tests.

3. RESULTS AND DISCUSSION

3.1 Synthesis of cationic polyaspartamides with controlled charge density

The charge density of cationic polymers affects their conformation and ability to interact with mucin. Therefore it is crucial to reveal the role of charges in the strength of mucoadhesion. Polyaspartamides provide a versatile chemical platform for testing the effect of different side groups on colloidal interactions, contrary to the limited structural variety of chitosan or polyacrylates used in the literature [6], [19]–[21], [44]. A large variety of polyaspartamides can be synthesised by adding different nucleophilic agents to polysuccinimide. Some of the cationic polyaspartamides with primary, secondary or tertiary amine side groups have been proven to be biocompatible [45] and are important candidates for excipients in mucoadhesive drug delivery. Here, novel cationic polyaspartamides with a controlled concentration of cationic side groups were designed to unravel the effect of side group composition on the properties of linear polyaspartamides and their interaction with mucin by various colloidal tools. Tertiary amine side groups were chosen as cationic functionality since reagents containing primary or secondary amine groups can form cross-links between polymer chains, so it would not be possible to separate the effect of charge density from molecular mass effects, or a complicated synthetic pathway would be required [12]. Some of the cationic polyaspartamides are prone to hydrolytic degradation, as reported earlier [41], which can also cause poorly defined molecular mass effects on the colloidal interactions with mucin. Considering all these aspects, we used 3-(dimethylamino)-propyl side groups (DMP) to synthesise polyaspartamides with sufficient aqueous stability and to avoid potential cross-linking side reactions. DMP was used in different ratios (25, 50, 75 or 100% of the repeating units) and the remaining succinimide units were reacted with ethanolamine to form neutral hydroxyethyl side groups (Scheme 1).

The chemical structure of the DMP-X polyaspartamides was confirmed by ^{1}H NMR spectroscopy. ^{1}H NMR spectra containing peak assignments shown in Figs. S1-S3. The side group ratio of DMP to all repeating units correlated strictly with the feed composition, and the maximum difference between them was less than 2% for each composition (Table 1.)

Table 1 Characterisation of the synthesised DMP-X polymers

Composition	$X_{DMP, NMR}$ (%)	$X_{DMP, potentiometry}$ (%)	pK_a (-)	Zeta potential (mV)	$d_{h, SEC}$ (nm)
DMP-100	98	100	9.0	11.4 ± 1.0	8.3
DMP-75	74	75	9.0	9.8 ± 2.7	7.4
DMP-50	51	50	9.2	8.3 ± 1.7	7.0
DMP-25	23	28	9.4	0.6 ± 1.0	6.5
DMP-0	0	-	-	-4.2 ± 3.9	6.2

$X_{DMP, NMR}$ is the molar percentage of DMP side groups of all repeating units determined from ^{1}H NMR spectrum; $X_{DMP, potentiometry}$ is the molar percentage of DMP side groups of all repeating units from potentiometric titrations. $d_{h, SEC}$ is the hydrodynamic radius estimated from SEC

3.2 Protonation state and zeta potential

The protonation state of tertiary amine side groups on polyaspartamides determines the charge density, thus the possible electrostatic interactions with mucin. Accordingly, the protonation was analysed by potentiometric titration. From the raw data (the potentiometric curves are shown in Fig. 1a) Bjerrum-type plots were calculated (Fig. 1b), which shows the protonation

rate as function of pH. All the cationic polymers are fully protonated at pH = 7.4, and their pK_a (Table 1) show a gradual decrease with the growing cationic side group (DMP) ratios that may be a result of the neighbouring group effect. A possible reason for the favourable deprotonation at high DMP content is the high intra-chain repulsion due to the densely packed cationic DMP groups [22]. A similar phenomenon was observed for anionic poly(aspartic acid) derivatives with different density of charged groups [45] DMP contents were also determined from potentiometric titration and showed strong correlation with the ^{1}H NMR results (Table 1).

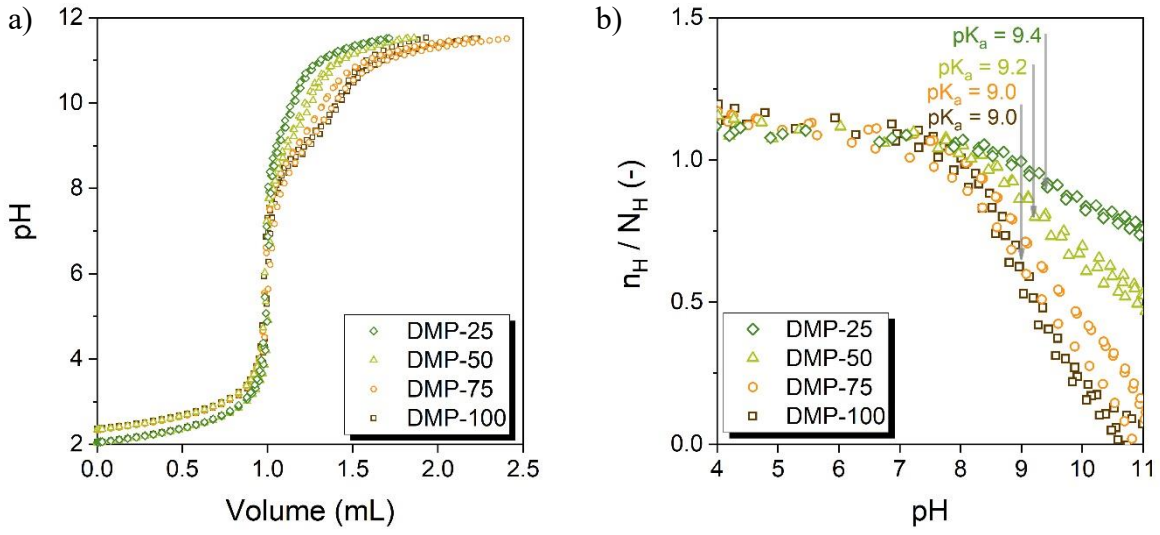

Fig. 1 a) Potentiometric titration and b) Bjerrum curves of DMP-X polymers, where n_H represents the molar amount of bound protons to the basic groups (-N(CH_3)$_2$) at the given pH, N_H is the molar amount of dissociable groups in the polymer

Zeta potential measurements provide complementary results to potentiometric data since they relate to the charge density of the moving macromolecule in solution. The zeta potential of the polymers was determined at pH 7.4 in PBS buffer (Table 1), where all the polymers were in their fully protonated state according to potentiometric data. DMP-100, DMP-75 and DMP-50 showed a positive zeta potential around 8–11 mV, while further reducing the DMP content a steep decrease was experienced. For DMP-25 the zeta potential is close to 0 mV, whereas for

the completely neutral DMP-0 a slightly negative value was measured, possibly due to the hydroxide ion adsorption on the neutral polyaspartamide. From these data, a non-linear behaviour of the polymers is expected with linearly increasing DMP content in electrostatic interactions with mucin.

The hydrodynamic volume and molecular mass of synthesised polyaspartamides were estimated using size exclusion chromatography (the chromatograms are shown in Fig. 2). Increasing the cationic side group content resulted in a gradual decrease in the elution volume, so an increase in the hydrodynamic radius was experienced with a linear dependence on the cationic side group content (Table 1, Fig. 2 a, b). These results suggest a gradual transformation of the polymer chains in solution from a random coil to a more extended conformation with increasing DMP content due to the intramolecular electrostatic repulsion of protonated side groups at pH = 7.4 [22]. It is worth mentioning that differences among the hydrodynamic radii of the polyaspartamides could not be detected by DLS (Fig. 2 c), and SEC proved to be more sensitive to size in this region. The molecular mass distribution of DMP-X polymers (Fig. 2 d) was determined from the result of neutral polyaspartamide (DMP-0) as the cationic derivatives might have a much higher charge density than conventional protein standards used for SEC measurements. The results are as follows for DMP-0: M_n = 71 kDa; M_w = 76 kDa; PDI = 1.07). The same chain length can be assumed for the cationic polyaspartamides, since they were synthesised directly from the same polysuccinimide batch, and no growth nor degradation is probable. The relatively high molecular mass values are specific for SEC measurements, other relative and absolute molecular mass-determining methods give smaller values for polyaspartamides. [41], [46].

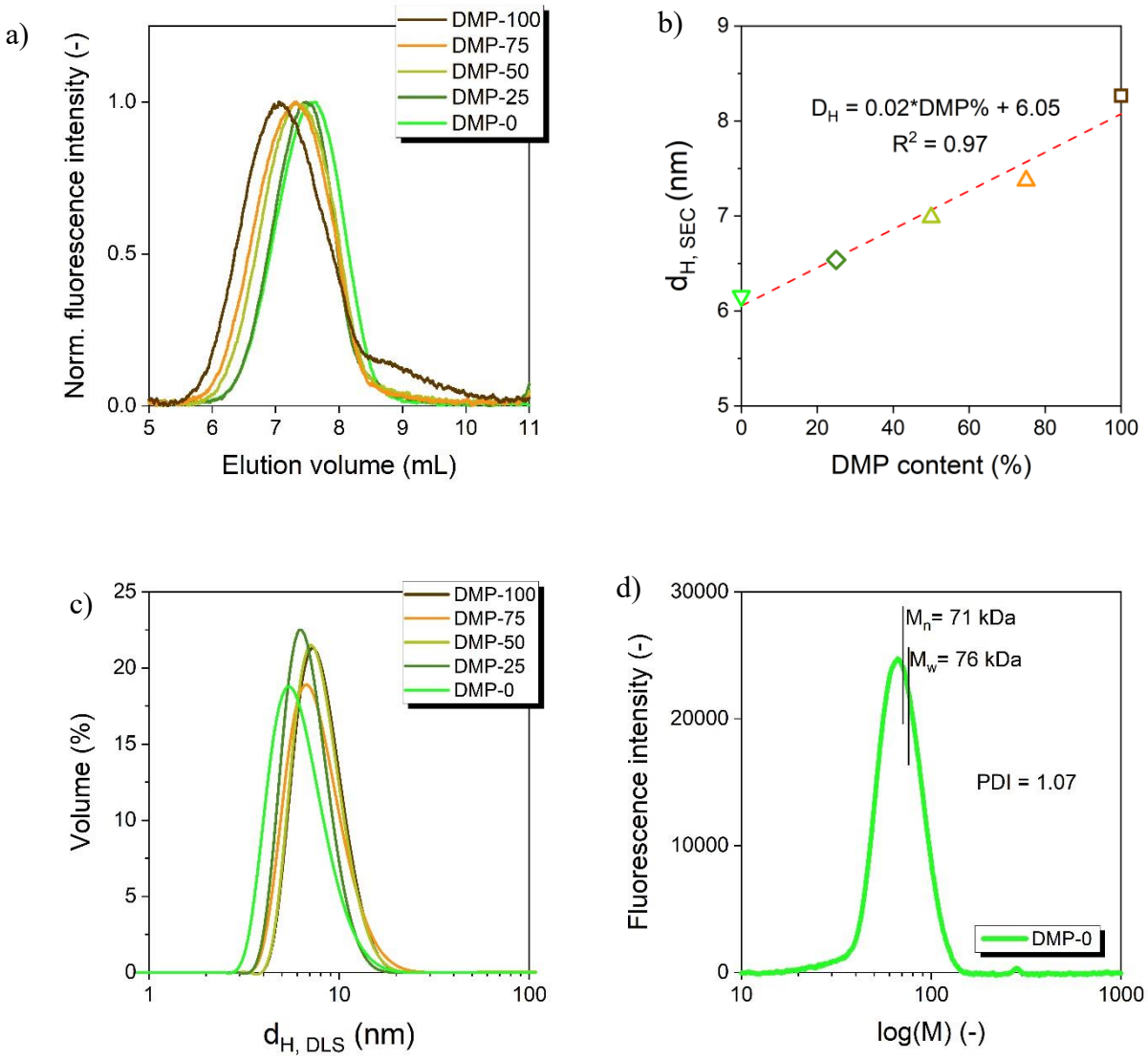

Fig. 2 a) Size exclusion chromatograms, b) calculated hydrodynamic diameters (form SEC) c) and distribution of hydrodynamic diameters (from DLS) of DMP-X polymers, d) molecular mass distribution of DMP-0 polymer

3.3 Biocompatibility, haemolysis assay

Haemolysis data is used as an indication of a possible toxic effect of polymers on cells. In this study, all cationic polymers as well as the neutral derivative showed negligible haemolytic effect, i.e., much below 10% of haemolysis caused by the positive control, Triton X-100 (Fig. 3), (lower than 1% compared to the negative control, $p \geq 0.05$) (ASTM F756-17) [47].

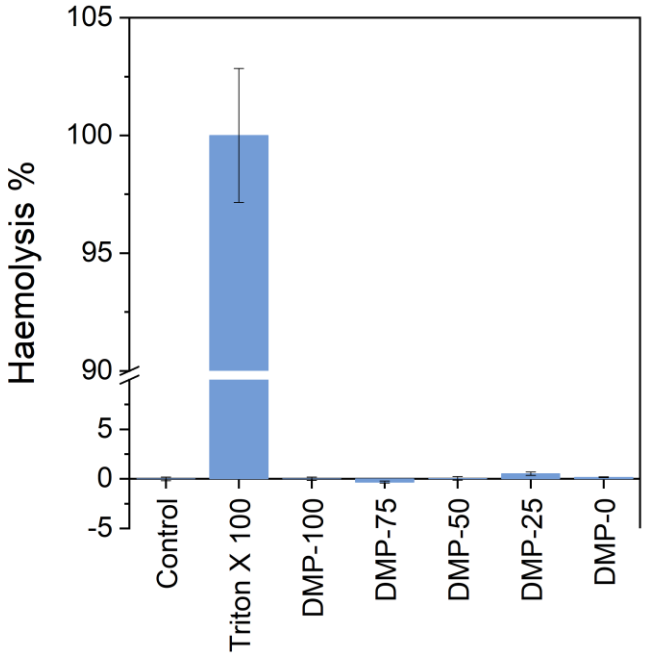

Fig. 3 Haemolysis assay of DMP-X polymers: the haemolytic effect is negligible for all studied polymers

Electrostatic interaction between cationic polyaspartamides and cell membranes [48] is expected, as reported previously in the literature between positively charged amine groups and the phosphate groups of the membranes. Nevertheless, according to our results, no significant adverse effect was detected in these polymers, which makes the polyaspartamides promising excipients in drug formulations. More importantly, the choice of cationic group content should not be based on biological safety issues, but the mucoadhesive performance of polymers can be the primary criterion as analysed in the next sections.

3.4 Polymer-induced aggregation of mucin in dispersion

Mucoadhesive interactions were probed by turbidimetric titration of mucin with polyaspartamides having different charge densities: a dilute aqueous dispersion of mucin particles was titrated with the solution of the polymer. The interaction between mucin and the

polymer at low polymer concentration (i.e., at low polymer-to-mucin mass ratio) is usually indicated by an increase in turbidity, generally quantified by the apparent absorbance at a chosen wavelength at which neither component has significant light absorbance, i.e., the change of absorbance is caused by light scattering. The increase in polymer concentration usually results in a maximum of turbidity followed by a gradual decrease as the polymer concentration is further increased. Khutoryanskiy et al. [10], [21] explained this with the formation of mucin aggregates as a result of the classical colloidal bridging effect of polymer molecules (e.g., chitosan) between mucin particles. At higher polymer concentrations, this bridging effect transforms into the coating of mucin particles by the polymer, and the particle size decreases to the size of the initial mucin aggregates.

Cationic polyaspartamides with a DMP content of 50% or higher brought about a strong increase in turbidity with increasing polymer-to-mucin mass ratio (polymer / mucin mass wt), indicating the possible aggregation of mucin (Fig. 4a). The titration curves of these compositions were evaluated, and the characteristic parameters suggested previously in the literature [49] were determined (Fig. 4b, Table 2). In general, the effect of the DMP content was proven to be significant ($p \leq 0.05$). Although, the polymer-to-mucin mass ratio at the initial increase could not be distinguished for these three compositions. The minor but significant ($p \geq 0.05$) differences in the other parameters indicates the importance of cationic group content at high charge densities. Turbidity at the initial increase was higher at higher DMP contents (significant difference between DMP-100 and DMP-50), similarly to the initial slope of the curves (significant difference between each polymer), indicating the enhanced ability of polyaspartamides with higher DMP content to induce mucin aggregation. A similar composition dependence was observed in the characteristic values of the maxima. The maximum value of turbidity also increased slightly (but not significantly) with the increasing DMP content (Fig. 4a and Table 2), and the corresponding polymer-to-mucin mass ratio

showed a minor shift to lower values with increasing DMP content (significant difference between DMP-50 and DMP-100, as well as DMP-75 and DMP-100). This can be explained by the fact that a lower amount of polymer is sufficient to form mucin aggregates. At the lower end of the composition scale, polyaspartamide with a DMP content of 25% (DMP-25) also caused some increase in turbidity, but no maximum was detected in the studied concentration range, and no characteristic points could be identified on the curve. Still, a slight and gradual increase of turbidity was detected, after which a plateau was reached, implying the presence of some interactions, although weaker than at higher DMP contents. Finally, the neutral polyaspartamide did not change the turbidity of the mucin dispersion, indicating the determining role of electrostatic interactions. Results of turbidimetric titration allow us to conclude that the effect of the charge density of DMP-X polyaspartamides interacting with mucin is not linear and monotonic, rather the charge density has a limit above which strong interactions can be formed. This information could be essential for the design of different polymer structures to optimise the strength of electrostatic interactions between cationic polymers and mucin.

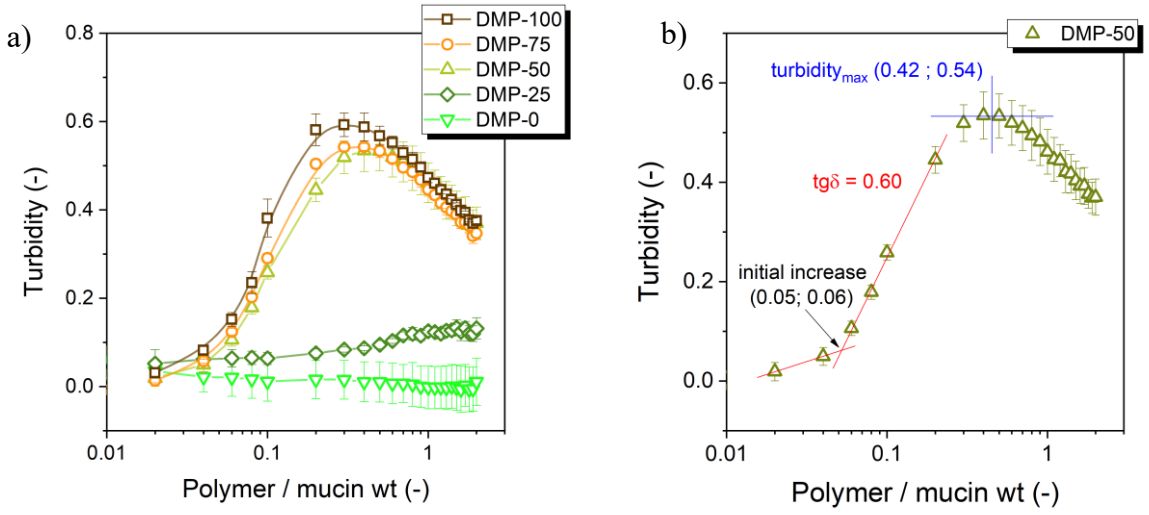

Fig. 4 a) Turbidimetric titration curves of DMP-X polymers interacting with mucin (all curves are corrected with a blank titration of mucin by polymer-free PBS solution), b) quantitative evaluation of the turbidity curve (DMP-50)

Table 2 DMP-X interaction with mucin, characteristic parameters from turbidimetric titration and zeta potential measurements

Composition	initial increase		tg δ	$turbidity_{max}$		charge reversal
	wt (-)	turbidity (-)	(-)	wt (-)	turbidity (-)	wt (-)
DMP-100	0.05	0.10	0.83	0.32	0.59	0.47
DMP-75	0.05	0.07	0.73	0.39	0.55	0.56
DMP-50	0.05	0.06	0.60	0.42	0.54	0.83

Where wt is the polymer-to-mucin mass ratio. An extended version of this table with standard deviation values for turbidimetric titration measurements can be found in the Supplementary Data (Table S1)

The interaction between DMP-X polymers and mucin was analysed in more detail by DLS and zeta potential measurements to verify that the electrostatic interaction is the main driving force of polymer-induced mucin aggregation. These sequential measurements allow us to follow the change of particle size distribution and zeta potential on the same sample. The general characteristics of DLS measurements are first presented on DMP-100 by the change of particle size distribution of mucin upon interaction with the polymer (Fig. 5a). The initial mucin dispersion is highly polydisperse (PDI = 0.40 – 0.50) but the volume-based particle size distribution remarkably changes to unimodal even at the lowest polymer/mucin mass ratio studied (wt = 0.1, PDI = 0.2 – 0.3). This phenomenon seems to contradict the theories in the literature [10], which propose polymer bridging between the initial mucin particles as the first step of the colloidal process. Considering that the change in scattered light intensity reaches its maximum and starts to decrease before the same happens with Z-average particle

size (Fig. 5b), a more complex mechanism can be hypothesised. We assume an initial rearrangement and homogenisation of the size of the mucin particles, and in parallel, the refractive index of the mucin particles may change upon polymer adsorption (Fig. 6. stage I to II). This process might be explained by the adsorption of polymer molecules even within the mucin particles resulting in the disintegration of loosely connected structures bound together by hydrophobic association. The hydration of the particles may also change as a result of electrostatic interactions between the polymer molecules and mucin, potentially causing the exclusion of some water and changing the refractive index of the particles. After this rearrangement step, aggregation occurs because the individual particles gradually lose their net negative charges due to the gradual adsorption of the cationic polymer (Fig. 6. stage II to III). These steps cannot be separated completely, as proven by the fact that the particle size itself slightly increases in the initial steps (at a low polymer-to-mucin mass ratio) (Fig. 5b). Therefore, a complex combination of processes can be assumed. as shown in Fig. 5c, the zeta potential gradually approaches zero with increasing polymer-to-mucin mass ratio, and the maximum particle size is reached at charge reversal. The adsorption of further cationic polymer molecules starts to disintegrate the aggregates stabilised by positive charges (Fig. 6. stage III to IV). As described above, the polymer-to-mucin mass ratio at charge reversal strictly coincides with the mass ratio at the maximum particle size of DMP-100 (Fig. 5c). A shift to higher mass ratios at charge reversal was experienced with decreasing DMP content (Fig. 5d) in agreement with the turbidity maxima (Table 2.). It is worth noting that the maximum particle size of mucin particles was similar for DMP-75 and DMP-50, and there is no clear difference in the corresponding mass ratios (Fig. 5e). Furthermore, the reduction of aggregate size is less pronounced at higher polymer-to-mucin mass ratios than for DMP-100. For DMP-25, a very similar tendency can be seen as in the turbidimetric titration with a slight increase in size with a plateau value at high polymer-to-mucin mass ratios. Accordingly,

charge reversal does not occur in the current concentration range supporting the decisive role of electrostatic interactions (Fig. 5d). Plotting the scattered light intensity from DLS measurements against the turbidity values of the given polymer-to-mucin mass ratios (Fig. 5 f), a reasonable correlation can be seen. However, there are visible differences as well. The intensity of scattered light reaches its maximum at lower polymer concentrations (0.2 for all polymers) than turbidity (mass ratios at the maximum vary between 0.32 and 0.42, see Table 2). Such difference can be explained by the non-equilibrium nature of the process and the fact that mucin aggregation strongly depends on the sample preparation pathway used (abrupt mixing of the components for DLS measurements vs step-wise addition of the titrant for turbidimetry [49]).

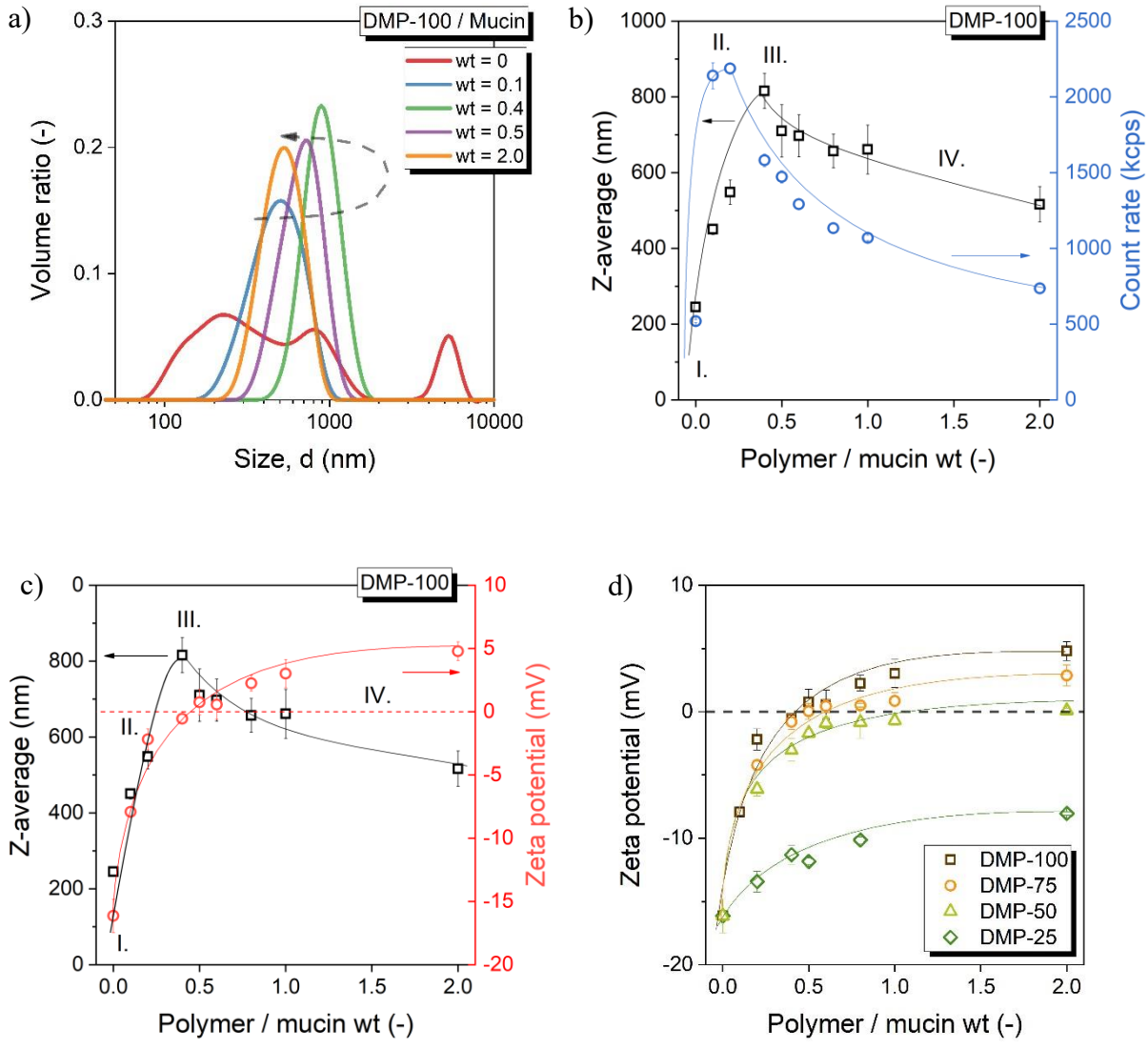

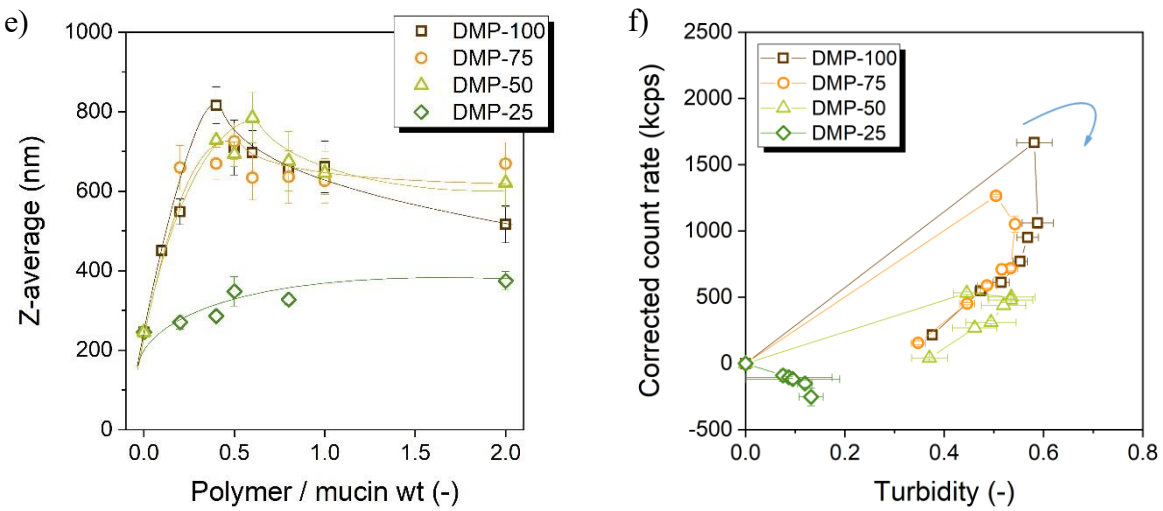

Fig. 5 Interaction of DMP-X polymers with mucin. DLS and zeta potential measurements for mixtures of mucin dispersions and polyaspartamide solutions. a) Change in particle size distribution at different polymer-to-mucin mass ratios (wt) (the dashed arrow shows the increase and subsequent decrease in particle size with increasing polymer-to-mucin mass ratio). b) Illustration showing the change in Z-average particle size and scattered light intensity from DLS measurements as a function of DMP-100-to-mucin mass ratio c) Illustration showing the change in Z-average particle size and zeta potential as a function of DMP-100-to-mucin mass ratio. d) Changes in the zeta potential of all compositions. e) Changes in the Z-average particle size of all compositions. f) Correlations between turbidity values and the corrected count rate of scattered light from DLS measurements (the corrected values are obtained by subtracting the data of the blank measurement of the mucin dispersion with PBS solution). The curved blue arrow shows the direction of the increase in the polymer-to-mucin mass ratio.

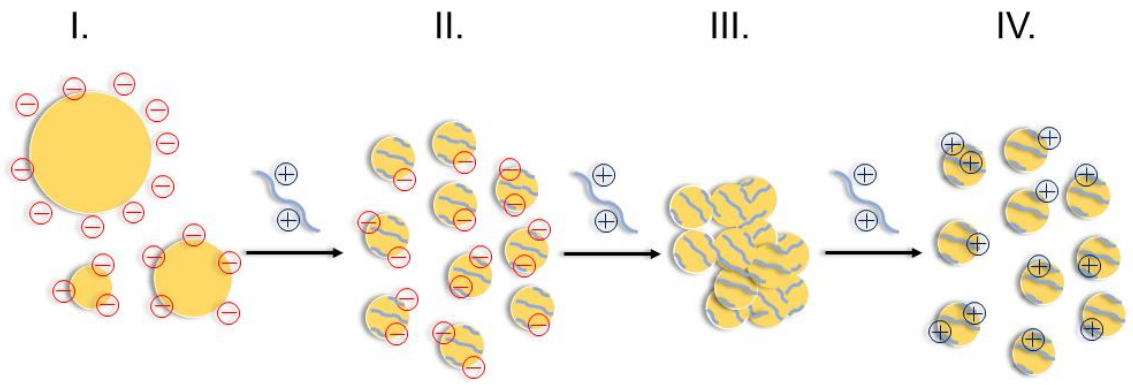

Fig. 6 Hypothesised process of mucin DMP-X interaction during colloidal measurements, where mucin particles are symbolised with yellow spheres and cationic polyaspartamides with curved blue lines. The net charge of mucin particles is indicated in each stage.

3.5 Polymer-mucin interaction in thin layer

A quartz crystal microbalance (QCM) was used as a quantitative tool to measure the adsorption of cationic polyaspartamides with different charge densities on mucin. Mucoadhesion in QCM methods is usually measured on a thin mucin layer deposited on the crystal surface [33], [35], [50], then an aqueous polymer solution flows through the cell used in the measurement. This experimental setup gives the opportunity to screen the interactions in rather 2D (on a flat surface), which is closer to life-like situations on the mucosal surfaces than the previously used 3D colloidal methods. Furthermore, QCM conditions can mimic the shear stress within the body contrary to the presence of only Brownian motion in 3D measurements.

The sequence of the adsorption process in the flow system with the data of a representative measurement (DMP-50) is shown in Fig. 7. First, the mucin was adsorbed on the crystal with some desorption in the subsequent rinsing step. Then, the given polyaspartamide was adsorbed on the mucin layer by flowing a dilute polymer solution (0.1 g L^{-1}) through the cell.

Finally, adsorption was tested with a more concentrated polymer solution as well (1 g L^{-1}), and a second rinsing step was applied to test the desorption of polymers.

The change of frequency and resistance values in QCM measurements (Table S2) were used to estimate the adsorbed mass and the consistency of the layer. The thickness of the mucin layer can be estimated from the amount of material deposited on the crystal surface. Considering the average change in mass calculated for mucin (~0.38 µg cm^{-2}), the estimated thickness was approximately 3-4 nm. This value is consistent with the AFM images of the uncovered and mucin-covered gold crystal surfaces (Fig. S4). The adsorption of mucin results in an obvious change in the morphology of the gold surface, reducing but not eliminating the roughness, as indicated by the data in Table S3. The changes in the resistance values upon adsorption (Table S2) suggest the loose layer structure of mucin, which might allow cationic polymers to reach deeper layers, not only the outer surface.

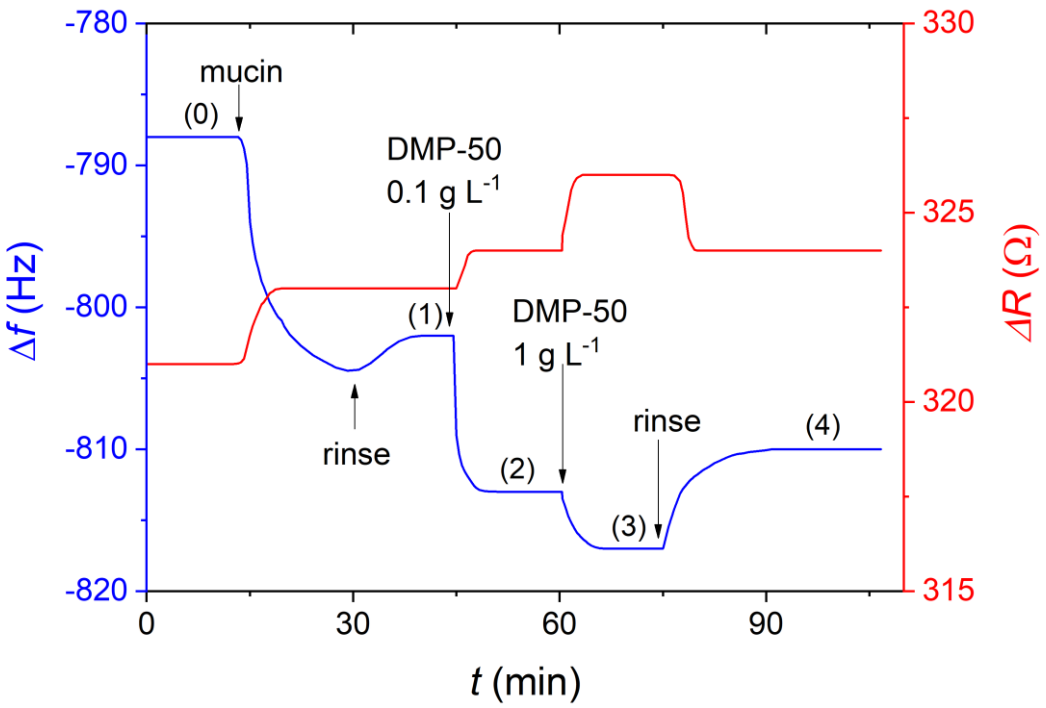

Fig. 7 The process of the QCM measurement can be seen on a curve recorded for DMP-50

Mucin-to-polymer mass ratios for the cationic polyaspartamides with different charge densities were calculated during the adsorption process (Fig. 8; raw data are shown in Table S2). Change in the resistance values, thus layer consistency, did not show a structure-dependent variation, but the frequency changes indicated a strong effect of cationic group content on adsorption and desorption processes. Furthermore, polyaspartamide adsorption on the mucin layer shows some unexpected trends compared to the results gained by 3D methods. First, only the neutral polyaspartamide showed negligible adsorption. All cationic polyaspartamides (DMP-25, DMP-50, DMP-75 and DMP-100) showed significant adsorption on mucin at both concentrations, but with remarkable differences (Fig. 8 and Fig. 9). In agreement with turbidimetric titration, both DMP-75 and DMP-50 showed a higher polymer-to-mucin mass ratio than DMP-100, even after the final rinsing step. Therefore, the highest cationic group content did not result in the highest adsorbed amount. Interestingly, DMP-25 showed a comparable adsorption before rinsing but a significant desorption was obtained and completely removed from the mucin surface. The effect of the stages and the DMP content during the experiment proved to be significant ($p \leq 0.05$) by repeated measures ANOVA. Post-hoc tests show significant differences between each experimental stage and in the effect of polymer composition between DMP-50 and DMP-25 as well as between DMP-50 and DMP-100. It can be concluded that more polymer molecules interact with the mucin layer at lower DMP content, which is consistent with the 3D colloidal measurements.

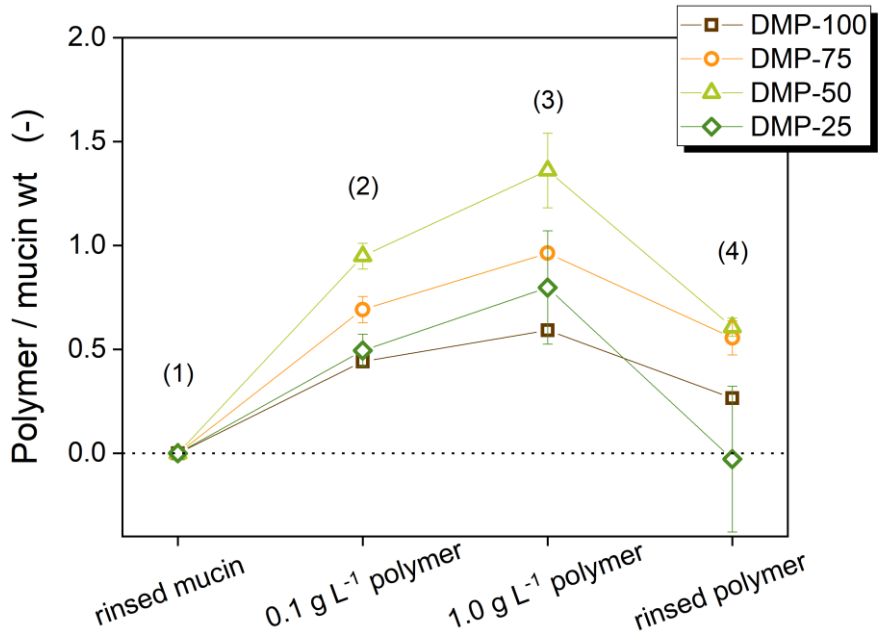

Fig. 8 The adsorbed mass ratio of DMP-X to mucin during QCM measurements. Data points are not shown for DMP-0 (no measurable adsorption)

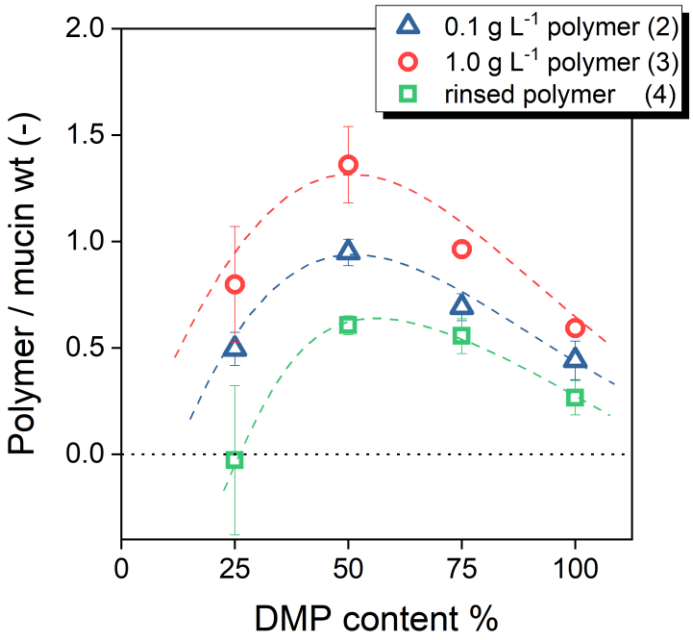

Fig. 9 The adsorbed mass ratio of DMP-X polymers to mucin as a function of DMP content in different stages of adsorption-desorption processes (see the processes in Fig. 7). Data points are not shown for DMP-0 (no measurable adsorption).

The correlations between the 3D and 2D methods are visualised in Fig. 10. Interestingly, the polymer-to-mucin mass ratios at charge reversal from the zeta potential measurement and the mass ratios of adsorbed polymer to mucin in a thin layer from the QCM method not only correlate, but even the numerical values of these completely different measurements are practically the same indicating the determining role of electrostatic interactions (Fig. 10a). We also found a linear correlation between the adsorbed amount of polymers at higher polymer concentration on a thin layer of mucin, and turbidimetry data suggesting similar colloidal processes behind the two results of the two measurements (Fig. 10b). However, it must be noted that QCM gives very valuable data on the possible desorption of polymers under flow conditions that cannot be obtained by the 3D methods.

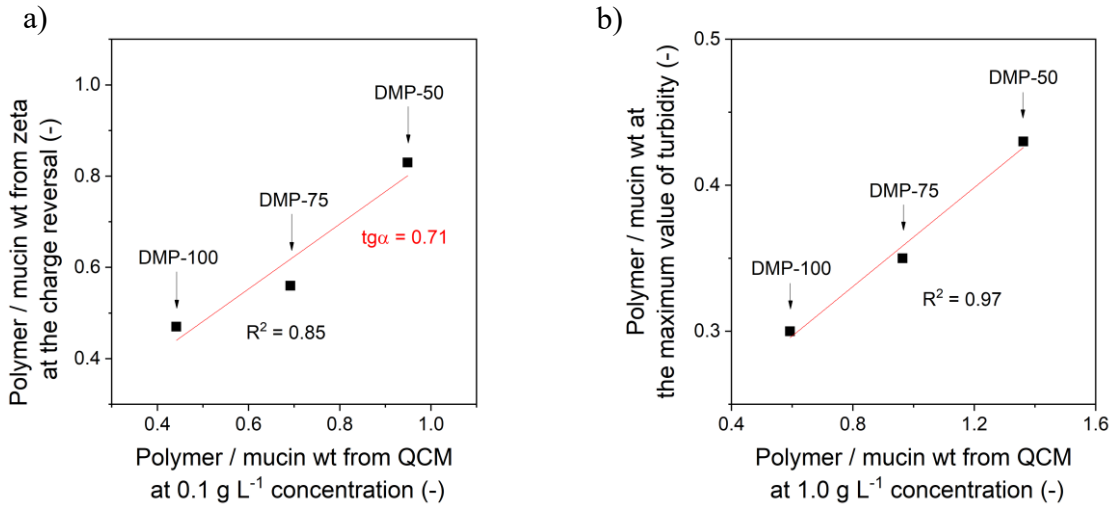

Fig. 10 Correlation between 3D and 2D measurements; a) correlation between QCM and zeta potential data for different polymers at lower polymer concentration, b) correlation between QCM and turbidimetry data for different polymers at higher polymer concentration.

In conclusion, lower charge densities are beneficial to adsorb higher amounts of polymer, but an optimum can be assumed as desorption is much more pronounced for DMP-25 and DMP-

50 and a minimum charge density is needed to overcome shear forces in a flow system or Brownian motion in case of colloidal measurements. The results also support that the maximum adsorbed amount should not be expected from the highest cationic group content (DMP-100) as the high DMP content causes a lower molar amount to adsorb; furthermore, high charge density might result in a more rigid structure that prohibits entanglements and interactions with mucin. Accordingly, the chemical composition should be optimised by taking into account both adsorption and desorption processes. Before cumbersome QCM measurements, simple colloidal methods can give valuable clues for potentially mucoadhesive structures.

4. CONCLUSION

We designed a series of cationic polyaspartamides with identical chain lengths, but various charge densities by changing the molar ratio of the cationic to neutral groups within the polymers. The chemical structure and side group content were confirmed by ^{1}H NMR spectroscopy. The concentration of cationic groups was also confirmed by potentiometric titration, which showed a slight composition-dependency of the pK_a values of cationic groups. Interestingly, zeta potential increased significantly only up to the cationic group content of 50%, suggesting the limited accessibility of cationic groups at high charge densities. The effect of the charge density of polyaspartamides on macromolecular polymer-mucin interactions was first tested through colloidal methods in dilute mucin dispersion, referred to as interactions in 3D. The polydispersity of mucin dispersion was remarkably reduced by adding cationic polyaspartamides, even at low polymer concentrations. In contrast, further addition of cationic polyaspartamides resulted in charge reversal and aggregation of mucin particles for the polymers containing 50% or more cationic groups. At high polymer-to-mucin ratios, the turbidity of the dispersions decreased, probably because of the de-aggregation process. However, the change of light scattering intensity did not strictly follow the change in particle size, suggesting the complexity of the colloidal processes. In accordance with the zeta potential of polyaspartamides, the increase of cationic group content above 50% caused only minor but monotonous changes in the turbidity of mucin dispersions. The polyaspartamide with only neutral side groups showed no colloidal changes indicating the electrostatic nature of interactions. In the second step of the study, a thin layer of mucin was deposited on quartz crystals and adsorption was tested on thin mucin layers in 2D using a quartz crystal microbalance (QCM). Again, no significant adsorption was obtained for polyaspartamides with neutral side groups, while polyaspartamides with 25% or higher cationic group content adsorbed efficiently on the mucin layer, although at 25% DMP content, the polymer was

completely removed by rinsing with PBS solution. Polyaspartamides containing 50 or 75% cationic side groups adsorbed in the highest amount, suggesting that the optimal composition is different from the completely cationic polymer derivative. We assume that an intermediate cationic group content could be the most beneficial to achieve strong interactions and a high adsorbed amount of polymer on mucin. The latter can also be affected by the increase in the hydrodynamic volume of polyaspartamides with increasing cationic group content. Interactions are not strong enough to withstand shear forces in flow mode experiments at low charge densities or without charged functional groups. In conclusion, QCM and conventional colloidal methods provide complementary results on the nature and strength of polymer-mucin interactions, making them valuable methods for testing the potential mucoadhesion of polymers. Nevertheless, the ranking of different polymers according to their mucoadhesive performance might be affected by the methods used and the type of the dosage form formulated from polymers. Therefore, these effects should be considered in future work. It was also shown that polyaspartamides are a remarkable chemical platform for examining the effect of type and concentration of chemical functionalities on mucin-polymer interactions. Furthermore, the cationic polyaspartamides studied here may be of great interest for mucosal drug delivery.

AUTHOR CONTRIBUTIONS

Gergely Stankovits: investigation, methodology, formal analysis, writing – original draft, visualization. Ágnes Ábrahám: methodology, investigation, formal analysis. Éva Kiss: conceptualization, methodology, resources. Zoltán Varga: investigation, formal analysis. Anil Misra: investigation, formal analysis. András Szilágyi: writing – review & editing, resources, funding acquisition. Benjámin Gyarmati: conceptualization, methodology, writing – review & editing, supervision, funding acquisition.

CONFLICTS OF INTEREST

The authors declare no competing financial interest.

ACKNOWLEDGEMENT

Project no. TKP-6-6/PALY-2021 has been implemented with the support provided by the Ministry of Culture and Innovation of Hungary from the National Research, Development and Innovation (NRDI) Fund, financed under the TKP2021-NVA funding scheme. Further support was provided by the NRDI Office via grant FK 138029. B. Gyarmati acknowledges the János Bolyai Research Scholarship of the Hungarian Academy of Sciences. The work was also supported by the ÚNKP-22-5 New National Excellence Program (ÚNKP-22-5-BME-297) of the Ministry for Innovation and Technology from the source of the NRDI Fund. G. Stankovits is grateful for the scholarship of the National Talent Programme of Hungary. The work was supported by the Lendület (Momentum) Programme of the Hungarian Academy of Sciences (Grant ID: LENDULET_2021-28). Project no. 2018-1.2.1-NKP-2018-00005 has been implemented with the support provided from the National Research, Development and Innovation Fund of Hungary, financed under the 2018-1.2.1-NKP funding scheme. These studies were supported by grant (VEKOP-2.3.3-15-2017-00020) from the European Union and the State of Hungary, co-financed by the European Regional Development Fund. The research was also funded by the H2020-MSCA-RISE-2016-–734641 NanoMed project. The authors thank Dávid Kun for his assistance with statistical analysis.

REFERENCES

[1] J. Das Neves, R. Sverdlov Arzi, and A. Sosnik, "Molecular and cellular cues governing nanomaterial-mucosae interactions: From nanomedicine to nanotoxicology," *Chemical Society Reviews*, vol. 49, no. 14. pp. 5058–5100, 2020. doi: 10.1039/c8cs00948a.

[2] R. Kulkarni, S. Fanse, and D. J. Burgess, "Mucoadhesive drug delivery systems: a promising non-invasive approach to bioavailability enhancement. Part I: biophysical considerations," *Expert Opin Drug Deliv*, pp. 1–18, Feb. 2023, doi: 10.1080/17425247.2023.2181331.

[3] K. Netsomboon and A. Bernkop-Schnürch, "Mucoadhesive vs. mucopenetrating particulate drug delivery," *European Journal of Pharmaceutics and Biopharmaceutics*, vol. 98, pp. 76–89, Jan. 2016, doi: 10.1016/J.EJPB.2015.11.003.

[4] S. Hu *et al.*, "A mussel-inspired film for adhesion to wet buccal tissue and efficient buccal drug delivery," *Nature Communications 2021 12:1*, vol. 12, no. 1, pp. 1–17, Mar. 2021, doi: 10.1038/s41467-021-21989-5.

[5] P. Schattling, E. Taipaleenmäki, Y. Zhang, and B. Städler, "A Polymer Chemistry Point of View on Mucoadhesion and Mucopenetration," *Macromolecular Bioscience*, vol. 17, no. 9. Wiley-VCH Verlag, Sep. 01, 2017. doi: 10.1002/mabi.201700060.

[6] H. T. Lam, O. Zupančič, F. Laffleur, and A. Bernkop-Schnürch, "Mucoadhesive properties of polyacrylates: Structure – Function relationship," *Int J Adhes Adhes*, vol. 107, Jun. 2021, doi: 10.1016/j.ijadhadh.2021.102857.

[7] Q. D. Pham, S. Nöjd, M. Edman, K. Lindell, D. Topgaard, and M. Wahlgren, "Mucoadhesion: mucin-polymer molecular interactions," *Int J Pharm*, vol. 610, Dec. 2021, doi: 10.1016/j.ijpharm.2021.121245.

[8] E. O. McGhee, S. M. Hart, J. M. Urueña, and W. G. Sawyer, "Hydration Control of Gel-Adhesion and Muco-Adhesion," *Langmuir*, vol. 35, no. 48, pp. 15769–15775, Dec. 2019, doi: 10.1021/acs.langmuir.9b02816.

[9] R. P. Brannigan and V. V. Khutoryanskiy, "Progress and Current Trends in the Synthesis of Novel Polymers with Enhanced Mucoadhesive Properties," *Macromolecular Bioscience*, vol. 19, no. 10. Wiley-VCH Verlag, Oct. 01, 2019. doi: 10.1002/mabi.201900194.

[10] V. v. Khutoryanskiy, "Advances in mucoadhesion and mucoadhesive polymers.," *Macromol Biosci*, vol. 11, no. 6, pp. 748–64, Jun. 2011, doi: 10.1002/mabi.201000388.

[11] B. Gyarmati, G. Stankovits, B. Á. Szilágyi, D. L. Galata, P. Gordon, and A. Szilágyi, "A robust mucin-containing poly(vinyl alcohol) hydrogel model for the in vitro characterization of mucoadhesion of solid dosage forms," *Colloids Surf B Biointerfaces*, vol. 213, May 2022, doi: 10.1016/j.colsurfb.2022.112406.

[12] B. Á. Szilágyi, A. Mammadova, B. Gyarmati, and A. Szilágyi, “Mucoadhesive interactions between synthetic polyaspartamides and porcine gastric mucin on the colloid size scale,” *Colloids Surf B Biointerfaces*, vol. 194, no. June, p. 111219, 2020, doi: 10.1016/j.colsurfb.2020.111219.

[13] M. Abdulkarim *et al.*, “Nanoparticle diffusion within intestinal mucus: Three-dimensional response analysis dissecting the impact of particle surface charge, size and heterogeneity across polyelectrolyte, pegylated and viral particles,” *European Journal of Pharmaceutics and Biopharmaceutics*, vol. 97, pp. 230–238, Nov. 2015, doi: 10.1016/j.ejpb.2015.01.023.

[14] I. Colijn *et al.*, “Colloidal dynamics of emulsion droplets in mouth,” *J Colloid Interface Sci*, vol. 620, pp. 153–167, Aug. 2022, doi: 10.1016/j.jcis.2022.03.117.

[15] A. R. Freitas *et al.*, “Modification of chicha gum: Antibacterial activity, ex vivo mucoadhesion, antioxidant activity and cellular viability,” *Int J Biol Macromol*, vol. 228, pp. 594–603, Feb. 2023, doi: 10.1016/j.ijbiomac.2022.12.204.

[16] V. Dinu *et al.*, “Mucin immobilization in calcium alginate: A possible mucus mimetic tool for evaluating mucoadhesion and retention of flavour.,” *Int J Biol Macromol*, vol. 138, pp. 831–836, Oct. 2019, doi: 10.1016/j.ijbiomac.2019.07.148.

[17] R. B. Qaqish and M. M. Amiji, “Synthesis of a fluorescent chitosan derivative and its application for the study of chitosan-mucin interactions,” *Carbohydr Polym*, vol. 38, no. 2, pp. 99–107, 1999, doi: 10.1016/S0144-8617(98)00109-X.

[18] Y. A. Albarkah, R. J. Green, and V. V. Khutoryanskiy, “Probing the Mucoadhesive Interactions between Porcine Gastric Mucin and Some Water-Soluble Polymers,” *Macromol Biosci*, vol. 15, no. 11, pp. 1546–1553, Nov. 2015, doi: 10.1002/mabi.201500158.

[19] I. A. Sogias, A. C. Williams, and V. V. Khutoryanskiy, “Why is Chitosan Mucoadhesive?,” *Biomacromolecules*, vol. 9, no. 7, pp. 1837–1842, Jul. 2008, doi: 10.1021/bm800276d.

[20] M. B. Stie, J. R. Gätke, F. Wan, I. S. Chronakis, J. Jacobsen, and H. M. Nielsen, “Swelling of mucoadhesive electrospun chitosan/polyethylene oxide nanofibers facilitates adhesion to the sublingual mucosa,” *Carbohydr Polym*, vol. 242, p. 116428, Aug. 2020, doi: 10.1016/j.carbpol.2020.116428.

[21] N. A. Fefelova, Z. S. Nurkeeva, G. A. Mun, and V. V. Khutoryanskiy, “Mucoadhesive interactions of amphiphilic cationic copolymers based on [2-(methacryloyloxy)ethyl]trimethylammonium chloride,” *Int J Pharm*, vol. 339, no. 1–2, pp. 25–32, Jul. 2007, doi: 10.1016/j.ijpharm.2007.02.019.

[22] M. Brynda, P. Chodanowski, and S. Stoll, “Polyelectrolyte-particle complex formation. Polyelectrolyte linear charge density and ionic concentration effects. Monte Carlo simulations,” *Colloid Polym Sci*, vol. 280, no. 9, pp. 789–797, 2002, doi: 10.1007/s00396-002-0705-0.

[23] P. M. Claesson, E. Poptoshev, E. Blomberg, and A. Dedinaite, “Polyelectrolyte-mediated surface interactions,” *Adv Colloid Interface Sci*, vol. 114–115, pp. 173–187, Jun. 2005, doi: 10.1016/J.CIS.2004.09.008.

[24] R. Podgornik and M. Ličer, “Polyelectrolyte bridging interactions between charged macromolecules,” *Curr Opin Colloid Interface Sci*, vol. 11, no. 5, pp. 273–279, Nov. 2006, doi: 10.1016/J.COCIS.2006.08.001.

[25] B. Demouveaux, V. Gouyer, F. Gottrand, T. Narita, and J. L. Desseyn, “Gel-forming mucin interactome drives mucus viscoelasticity,” *Advances in Colloid and Interface Science*, vol. 252. Elsevier B.V., pp. 69–82, Feb. 01, 2018. doi: 10.1016/j.cis.2017.12.005.

[26] L. Sardelli *et al.*, “Towards bioinspired: In vitro models of intestinal mucus,” *RSC Advances*, vol. 9, no. 28. Royal Society of Chemistry, pp. 15887–15899, 2019. doi: 10.1039/c9ra02368b.

[27] Y. A. Albarkah, R. J. Green, and V. V. Khutoryanskiy, “Probing the Mucoadhesive Interactions between Porcine Gastric Mucin and Some Water-Soluble Polymers,” *Macromol Biosci*, vol. 15, no. 11, pp. 1546–1553, 2015, doi: 10.1002/mabi.201500158.

[28] Á. Ábrahám, F. Massignan, G. Gyulai, M. Katona, N. Taricska, and É. Kiss, “Comparative Study of the Solid-Liquid Interfacial Adsorption of Proteins in Their Native and Amyloid Forms,” *Int J Mol Sci*, vol. 23, no. 21, Nov. 2022, doi: 10.3390/ijms232113219.

[29] Á. Ábrahám, M. Katona, G. Kasza, and É. Kiss, “Amphiphilic polymer layer – Model cell membrane interaction studied by QCM and AFM,” *Eur Polym J*, vol. 93, pp. 212–221, Aug. 2017, doi: 10.1016/j.eurpolymj.2017.05.047.

[30] A. K. Dutta, A. Nayak, and G. Belfort, “Viscoelastic properties of adsorbed and cross-linked polypeptide and protein layers at a solid-liquid interface,” *J Colloid Interface Sci*, vol. 324, no. 1–2, pp. 55–60, Aug. 2008, doi: 10.1016/j.jcis.2008.04.065.

[31] B. Jachimska, S. Świątek, J. I. Loch, K. Lewiński, and T. Luxbacher, “Adsorption effectiveness of β-lactoglobulin onto gold surface determined by quartz crystal microbalance,” *Bioelectrochemistry*, vol. 121, pp. 95–104, Jun. 2018, doi: 10.1016/j.bioelechem.2018.01.010.

[32] D. Migoń, T. Wasilewski, and D. Suchy, “Application of QCM in Peptide and Protein-Based Drug Product Development,” *Molecules*, vol. 25, no. 17. MDPI AG, Sep. 01, 2020. doi: 10.3390/molecules25173950.

[33] M. Marczynski, B. N. Balzer, K. Jiang, T. M. Lutz, T. Crouzier, and O. Lieleg, “Charged glycan residues critically contribute to the adsorption and lubricity of mucins,” *Colloids Surf B Biointerfaces*, vol. 187, Mar. 2020, doi: 10.1016/j.colsurfb.2019.110614.

[34] S. Oh, M. Wilcox, J. P. Pearson, and S. Borrós, “Optimal design for studying mucoadhesive polymers interaction with gastric mucin using a quartz crystal microbalance with dissipation (QCM-D): Comparison of two different mucin

origins," *European Journal of Pharmaceutics and Biopharmaceutics*, vol. 96, pp. 477–483, Oct. 2015, doi: 10.1016/j.ejpb.2015.08.002.

[35] S. Oh and S. Borrós, "Mucoadhesion vs mucus permeability of thiolated chitosan polymers and their resulting nanoparticles using a quartz crystal microbalance with dissipation (QCM-D)," *Colloids Surf B Biointerfaces*, vol. 147, pp. 434–441, Nov. 2016, doi: 10.1016/j.colsurfb.2016.08.030.

[36] A. Mammadova, B. Gyarmati, K. Sárdi, A. Paudics, Z. Varga, and A. Szilágyi, "Thiolated cationic poly(aspartamides) with side group dependent gelation properties for the delivery of anionic polyelectrolytes," *J Mater Chem B*, vol. 10, no. 31, pp. 5946–5957, Jun. 2022, doi: 10.1039/d2tb00674j.

[37] K. Molnar *et al.*, "Poly(amino acid) based fibrous membranes with tuneable in vivo biodegradation," *PLoS One*, vol. 16, no. 8 August, Aug. 2021, doi: 10.1371/journal.pone.0254843.

[38] K. Tóth *et al.*, "Characterization of Electrospun Polysuccinimide-Dopamine Conjugates and Effect on Cell Viability and Uptake," *Macromol Biosci*, Mar. 2023, doi: 10.1002/mabi.202200397.

[39] S. S. Gupta, V. Mishra, M. Das Mukherjee, P. Saini, and K. R. Ranjan, "Amino acid derived biopolymers: Recent advances and biomedical applications.," *Int J Biol Macromol*, vol. 188, pp. 542–567, Oct. 2021, doi: 10.1016/j.ijbiomac.2021.08.036.

[40] E. Krisch *et al.*, "Composite beads of silica gel, alginate and poly(Aspartic acid) for the immobilization of a lipase enzyme," *Express Polym Lett*, vol. 13, no. 6, pp. 512–523, Jun. 2019, doi: 10.3144/expresspolymlett.2019.43.

[41] B. Gyarmati *et al.*, "Side group ratio as a novel means to tune the hydrolytic degradation of thiolated and disulfide cross-linked polyaspartamides," *Polym Degrad Stab*, vol. 188, p. 109577, Jun. 2021, doi: 10.1016/j.polymdegradstab.2021.109577.

[42] "QCM200 Operation and Service Manual." pp. 15–15. Accessed: Mar. 22, 2023. [Online]. Available: https://www.thinksrs.com/downloads/PDFs/Manuals/QCM200m.pdf

[43] U. Latif, S. Can, O. Hayden, P. Grillberger, and F. L. Dickert, "Sauerbrey and anti-Sauerbrey behavioral studies in QCM sensors-Detection of bioanalytes," *Sens Actuators B Chem*, vol. 176, pp. 825–830, 2013, doi: 10.1016/j.snb.2012.09.064.

[44] T. M. M. Ways, W. M. Lau, and V. V. Khutoryanskiy, "Chitosan and its derivatives for application in mucoadhesive drug delivery systems," *Polymers*, vol. 10, no. 3. MDPI AG, Mar. 05, 2018. doi: 10.3390/polym10030267.

[45] C. Németh, B. Gyarmati, T. Abdullin, K. László, and A. Szilágyi, "Poly(aspartic acid) with adjustable pH-dependent solubility," *Acta Biomater*, vol. 49, pp. 486–494, Feb. 2017, doi: 10.1016/j.actbio.2016.11.065.

[46] R. Mendichi, G. Giammona, G. Cavallaro, and A. Giacometti Schieroni, "Molecular characterization of α,β-poly[(N -hydroxyethyl)- dl –aspartamide] by

light scattering and viscometry studies," *Polymer (Guildf)*, vol. 41, no. 24, pp. 8649–8657, Nov. 2000, doi: 10.1016/S0032-3861(00)00185-3.

[47] "Standard Practice for Assessment of Hemolytic Properties of Materials, Annual Book of ASTM Standards", ASTM F756-00, Vol. 13.01, 2010 doi: 10.1520/F0756-17.

[48] E. F. Palermo, D. K. Lee, A. Ramamoorthy, and K. Kuroda, "Role of cationic group structure in membrane binding and disruption by amphiphilic copolymers," *Journal of Physical Chemistry B*, vol. 115, no. 2, pp. 366–375, Jan. 2011, doi: 10.1021/jp1083357.

[49] Y. A. Antonov, P. Moldenaers, and R. Cardinaels, "Binding of lambda carrageenan to bovine serum albumin and non-equilibrium effects of complexation," *Food Hydrocoll*, vol. 126, May 2022, doi: 10.1016/j.foodhyd.2021.107321.

[50] S. Oh, M. Wilcox, J. P. Pearson, and S. Borrós, "Optimal design for studying mucoadhesive polymers interaction with gastric mucin using a quartz crystal microbalance with dissipation (QCM-D): Comparison of two different mucin origins," *European Journal of Pharmaceutics and Biopharmaceutics*, vol. 96, pp. 477–483, Oct. 2015, doi: 10.1016/j.ejpb.2015.08.002.